Catalysis Communications 28 (2012) 58–63

Contents lists available at SciVerse ScienceDirect

Catalysis Communications

journal homepage: www.elsevier.com/locate/catcom

Short Communication

Facile synthesis of mesoporous bicrystallized TiO_2(B)/anatase (rutile) phases as active photocatalysts for nitrate reduction

Mohamed Mokhtar Mohamed *, B.H.M. Asghar, H.A. Muathen

Chemistry Department, Faculty of Science, Benha University, Benha, Egypt
Faculty of Applied Science, Umm Al-Qura University, Makkah, Saudi Arabia

ARTICLE INFO

Article history:
Received 7 May 2012
Received in revised form 28 July 2012
Accepted 13 August 2012
Available online 18 August 2012

Keywords:
Nitrate photoreduction
Polymeric templates
Bicrystalline TiO_2 (B)/anatase
Characterization

ABSTRACT

Polyhedral and wormhole-like mesoporous titania nanoparticles composed of TiO_2(B) and anatase (rutile) were successfully synthesized by hydrothermal self-assembly method employing, respectively polyacrylamide (AA), polyvinyl alcohol (VA) and polyoxyethyl lauryl ether (ELE) as templates. TEM, X-ray diffraction, FTIR, UV–vis DR spectroscopy and N_2 sorptiometry were used for the characterization of surface morphology, phase composition, electronic properties and surface texturing of the synthesized catalysts. The photocatalytic activity was evaluated via the photo-reduction of nitrate in aqueous solution under UV light irradiation. The TiO_2 catalyst derived from ELE presented the highest activity due to the alternate structure of anatase and TiO_2(B) phases.

1. Introduction

Agricultural effluents and sewage result in excessive amounts of nitrate in water supplies. High levels of nitrate in domestic water cause cyanosis in young babies and serious human health problems such as cancer [1]. The WHO standards advocate that NO_3^- in drinking water should be less than 50 mg/l [2]. Recently, the removal of nitrate is typically obtained using reverse osmosis, ion exchange and electrodialysis that are considered as expensive processes because of construction and management costs. Initial studies involving titania modified by metals (including Cu, Ag [3,4], Pt [5], and Ru [6]) and the use of dopant ions including $Fe^{3+}$and Cr^{3+} had shown poor selectivity towards nitrogen and only when mixed metals were employed the selectivity to nitrogen improve [3,7].

Three popular polymorphs of TiO_2 found in the nature are the anatase (tetragonal) [8], rutile (tetragonal) [8], and brookite (orthorhombic) phases [9]. Besides these phases, recently TiO_2(B) phase attracts great attention due to its unique crystallographic structure [10–12]. Because of the unique electronic properties of TiO_2(B), some of these composites have shown excellent photocatalytic activity even better than P25 [13]. However, to the best of our knowledge, few works employ short-time annealing methods to form a composite semiconductor with a bicrystalline structure. While bicrystalline products with anatase and TiO_2(B) have been explored, the photoactivity of these samples is still limited even under UV irradiation [12].

In this work, mesoporous TiO_2 nanoparticles (NP) of bicrystalline structure composed of TiO_2(B)/anatase(rutile) have successfully been synthesized; using a facile polymeric-assisted hydrothermal process, with desired structures and properties. The produced materials were characterized by various techniques including TEM, XRD, UV–vis DRS, N_2 sorptiometry, and FTIR spectrometry and then tested for nitrate reduction photocatalytically from aqueous solution. The catalytic activity and selectivity influenced by the effect of the support (morphology and texturing properties) as well as hole scavenger are also discussed.

2. Experimental

2.1. Synthesis of titania

Titania synthesized catalysts were prepared using various templates including polyoxyethyl lauryl ether (Ti_{PELE}), polyvinyl alcohol (Ti_{PVA}) and polyacrly amide (Ti_{PAA}) under hydrothermal conditions using tetra-isopropyl orthotitanate [$Ti(O\text{-}i\text{-}Pr)_4$] as a titanium source. The template was first dissolved in a mixture of ethanol and water (1:8 in volume) and then poured into a definite amount of orthotitanate followed by gradual stirring at room temperature until complete hydrolyzing of titanate. To stabilize the Ti precursor, pH of the solution was adjusted to 0.7 by nitric acid. After stirring, the mixture was then transferred into Teflon lined autoclave and heated hydrothermally at 373 K for two days followed by precipitate collection, washing with distilled water and drying at 393 K. Finally the synthesized materials were calcined at 623 K for 4 h to produce TELE, TVA and TAA samples denoted respectively, as Ti_{PELE}, Ti_{PVA} and Ti_{PAA}. TiO_2 P25 (70% anatase:30%rutile) with a surface area of 49 $m^2\ g^{-1}$ and primary crystal size 30 nm was purchased from Degussa for comparison purposes.

* Corresponding author. Tel.: +966 500969808; fax: +966 5501000.
E-mail address: mohmok2000@yahoo.com (M.M. Mohamed).

1566-7367/$ – see front matter
http://dx.doi.org/10.1016/j.catcom.2012.08.012

2.2. Catalyst characterization

The X-ray powder diffraction patterns of various solids were carried out using a Philips 321/00 instrument for the phase composition of the samples. The morphologies were studied by TEM micrographs (Philips; model Tecani Feil2). UV–vis diffuse reflectance spectra of various samples in the 800–200 nm range were obtained using a Jasco V-570 spectrophotometer with using $BaSO_4$ as a standard. FT-IR spectra of the samples, on KBr pellets, were recorded with a JASCO single beam FT-IR 5300-spectrometer. The thermograms of the synthesized samples were determined in an equipment SDT Q600 modulus of TA instruments. The surface properties namely BET surface area, total pore volume (Vp) and mean pore radius (r) were determined from N_2 adsorption isotherms measured at 77 K using a Micromeritics ASAP 2020 analyzer.

2.3. Photocatalytic reduction of nitrate

Batch photocatalytic experiments were performed using a 100 ml cylindrical Pyrex reaction vessel (10.0 cm diameter, 15 cm height) as the photoreactor. Water sample (50 ml) was taken as synthetic ones. A 125 W high pressure Hg lamp emitting radiation at 365 nm was used as the light source. The photoreactor was illuminated from the top and the mixture was slowly mixed by a magnetic stirrer to attain a homogeneous suspension. The solution (100 ppm NO_3^-) was left for 60 min before the illumination step to ensure complete adsorption. Formic acid was used as a hole scavenger that attained at 0.06 M. Prior to analytical measurements and after photocatalytic reduction experiments, the samples were filtered through 0.2 μm membrane filters (Millipore) to remove TiO_2 particles. The efficiency of photocatalytic process was investigated for photocatalyst loading at 0.1 g and for reaction periods of 5–13 h irradiation time. NO_2^- and NO_3^- analyses were performed by ion chromatography (861 Advance IC, Metrohm). To measure the ammonium concentration, H_2SO_4 was added to the sample solution to prevent the release of ammonia gas and measured using the ion chromatograph equipped with a CS-15 column. The amount of H_2 produced was analyzed with an online TCD gas chromatograph (Shimadzu, GC-8A).

3. Results and discussion

3.1. Phase, morphology and optical properties

A broad diffraction peak at $2\theta = 0.9°$ is depicted following calcinations at 623 K in the small angel region to confirm mesoporous TiO_2 formation via various templates used (see Supplementary data). Fig. 1 describes the change of formation of anatase and rutile phases in the WXRD besides TiO_2(B) phase (JCPDS 46-1238, monoclinic, space group C2/m) as a function of annealing temperature. For the samples heated at 393 K, the TiO_2(B) phase was perceived as a quite broad band at $2\theta = 14.02°$ [14] reflecting its poor crystallinity together with another crystalline anatase phase. Following annealing at 623 K, the diffraction peaks were identified mainly as anatase in a well crystallized form with significant amounts of TiO_2(B) phase. The TiO_2(B) phase was maintained up to 623 K, but its crystallinity was slightly diminished, even though other crystalline peaks were evolved including the rutile phase; as in TVA sample. Summarized in Table 1 are the phase contents determined from the integrated XRD peak intensities of anatase (101), rutile (110), and TiO_2B (001) by a numerical deconvolution method [15]; also listed are the crystallite sizes calculated by Scherrer equation. Table 1 also indicates that the meta-stable anatase is the dominant phase for all the samples except the TVA one; which showed dominance of TiO_2(B) with minor phases of rutile and anatase. Evidently, increasing the annealing temperature into 623 K seems to encourage the phase transformation from TiO_2(B) into anatase and rutile. Both TVA and TAA samples presented the highest TiO_2(B) ratios (41–48%) where TELE indicated the lowest one (33.3%).

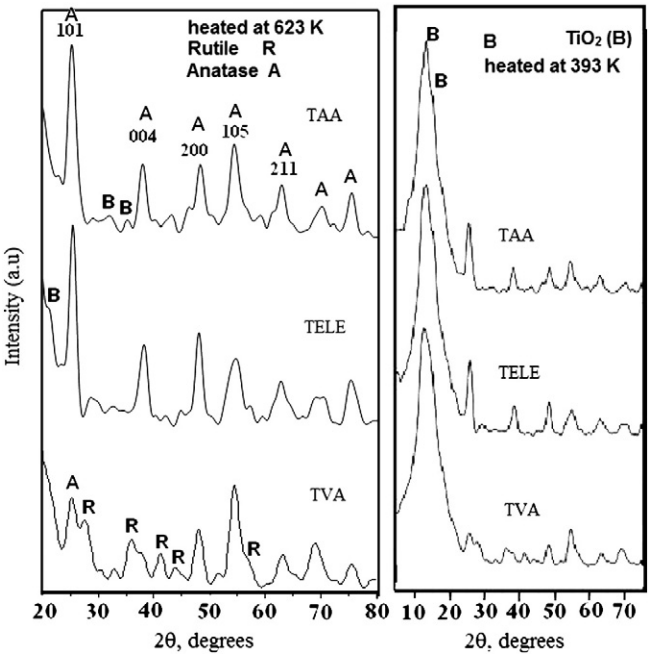

Fig. 1. WXRD patterns for the TiO_2(B), anatase (A) and rutile (R) phases obtained from hydrolysis of titanium isopropoxide with polyacrylamide (TAA), polyvinyl alcohol (TVA) and polyoxyethyl lauryl ether (TELE) under ethanol and acidic (HCl) water concentration autoclaved under hydrothermal conditions at 373 K for 2 days and heated independently at 393 K and 623 K for 5 h.

The TEM images of TVA and TAA where the mean particle sizes are close to 9 and 10 nm, respectively, show polyhedral structures dominated by truncated pentahedral and tetrahedral shapes (see Supplementary data). On the contrary, the TELE sample (Fig. 2) produced a disordered wormhole-like pore structure with diameters as small as 5 nm and a well uniform length within 13–15 nm. This micrograph demonstrates that the mesoporous structure consists of short worm-like mesoporous channel interconnected in 3D disordered way. On the other hand, a local HRTEM image (Fig. 2-inset) in the marked region revealed the presence of TiO_2(B) lattice spacing in line with the lattice fringes of the anatase with distances at 0.62 nm and 0.36 nm correspond to (102) and (101) planes of TiO_2(B) and anatase phases, respectively [16].

Fig. 3 shows the UV–vis diffuse reflectance spectra of prepared TiO_2 materials. The visible-light absorption of these photocatalysts was in the order of TAA > TELE ≈ TVA.

The prepared materials exhibit new optical properties apart from those of conventionally prepared TiO_2 exploring the probability of point defects and its effect on the band gap narrowing that governs the light absorption in the visible region [14]. The samples showed three absorption onsets at 283, 352 and 550 nm for all samples. Samples TELE and TVA showed another absorption onset at 385 nm. The presence of absorbance shoulder in the visible-light region was observed in all samples at 584 nm (TAA) and 574 nm (TELE, TVA). Displaying such a broad band, let us presume that it is due to broad distribution of Ti environments [17] that exhibits $E_g \sim 2.12$ eV. Medium shifts in the maximum values (ca. 10 nm), which are observed for TAA and TELE following calcinations could be consistent with average changes in the coordination environment of Ti species.

IR indicates that the bulk template residue has not been completely removed from the powder samples in the 1100–2500 cm^{-1} range (see Supplementary data) following calcinations at 623 K and a relatively strong peak at 1630 cm^{-1} due to deformation mode of H_2O groups is depicted. Accordingly, it is expected that some of the

Table 1
Characterization of the composition and morphology of the crystalline phases of TiO_2, synthesized using various templates, as determined from XRD analysis.

Material name	Template chemical formula	Template type	Anatase Crystallites size nm (contents)	Rutile Crystallites size nm (contents)	TiO_2(B) Crystallites size nm (contents)
TVA	C_2H_4O 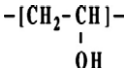	Non-ionic	12(32%)	10(20%)	4(48%)
TELE	$C_{12}H_{25}O(CH_2CH_2O)_4H$ 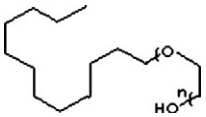	Non-ionic	20(61.4%)	(5.3%)	6(33.3)
TAA	C_3H_5NO 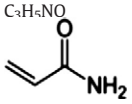	Anionic	15(58.4%)	–	10(41.6)

Note: The mean fraction of rutile (X_r) and anatase in the crystal lattice is calculated respectively based on the relationship between the integrated intensities of anatase (101) and rutile (121) peaks using the formulas in [19,21]; whereas that of TiO_2(B) is depicted using the $X_B = 1/1 + K(I_B/I_A)$ formula in which I_B represents (001) of TiO_2(B) and I_A equal (101) of anatase. The crystallite sizes of the resultant titania phases are estimated by the Scherrer's formula: $D(hkl) = K1\lambda/(\beta 1/2 \cos\theta)$.

obtained results from UV–vis spectra may partly be caused by the non-decomposed templates that indeed will take part in the reaction.

3.2. Porosity characterization

The adsorption–desorption isotherms are of type IV, according to the IUPAC classification [18]. A clear hysteresis at high relative pressure is observed, justifying capillary condensation of H_1 type. The isotherms and pore size distribution as calculated from the adsorption branch of the isotherm are shown in Fig. 4a, b. The pore size distribution of TVA (TAA) shows a bimodal distribution with maxima at 20 Å (sharp) and at 90 (sharp) Å, where that of TELE indicates distribution at 20 Å and 125 Å (broad). These bands are thought to correspond, respectively to the inner diameter of the nanoparticles and to the voids caused by its aggregation processes. The BET surface area (129.9 m^2/g) and total pore volume (0.4103 cm^3/g) of TELE exceed those of TVA (106.7 m^2/g, 0.3647 cm^3/g) and TAA (104.3 m^2/g, 0.3723 cm^3/g) where the pore radius of the former (14.1 nm) was found to decline compared with

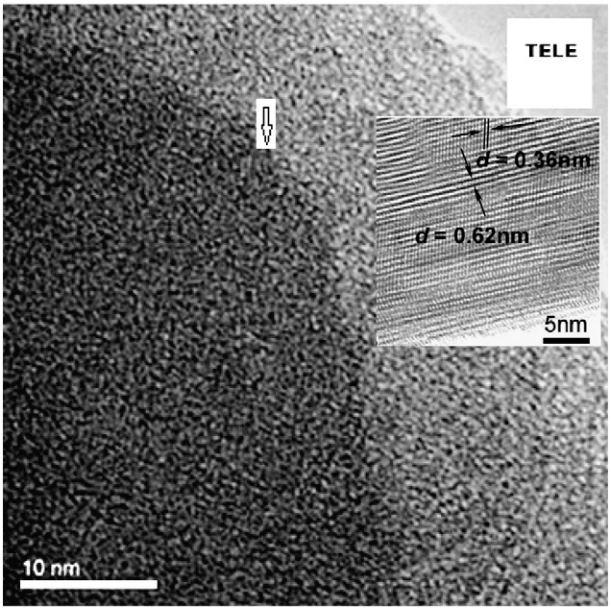

Fig. 2. TEM image of mesoporous TiO_2 derived from the ELE template and in-set HRTEM image of the worm marked in the large image.

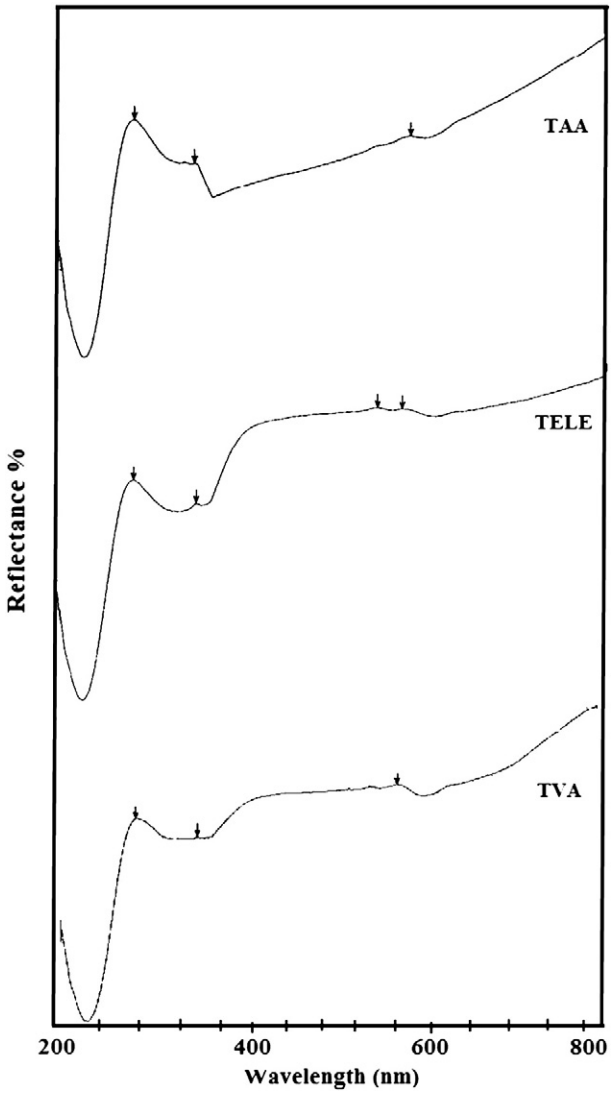

Fig. 3. UV–vis spectra of mesoporous titania samples.

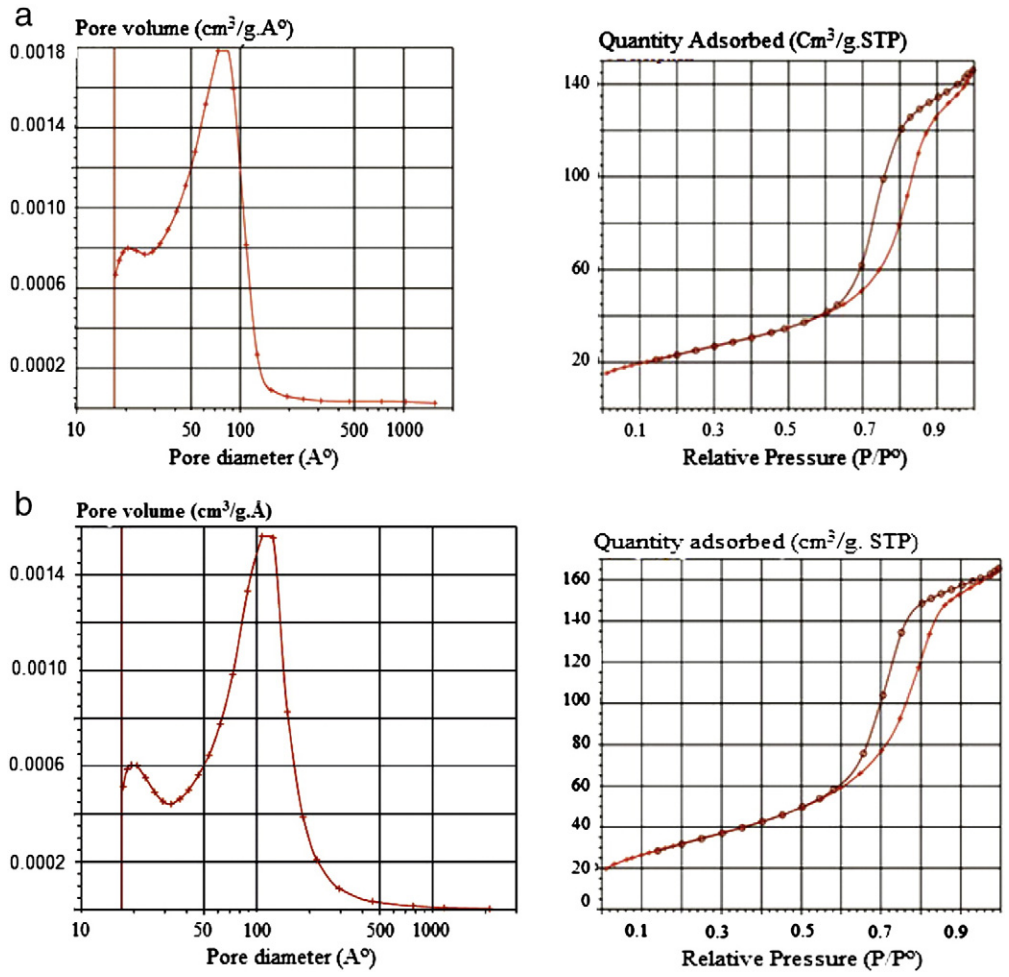

Fig. 4. a. N_2 adsorption/desorption isotherm and BJH adsorption dV/dD pore volume for TAA sample. b. N_2 adsorption/desorption isotherm and BJH adsorption dV/dD pore volume for TELE sample.

those of later proposing that the pores synthesized using polyoxyethyl lauryl ether were deep but not wide. Thus, evidently the long chain polyoxyethyl lauryl ether possesses a detrimental effect on surface area and pore volume values as compared with those of short chain polyvinyl alcohol and polyacrylamide surfactants.

3.3. Photocatalytic reduction of nitrates

In the system containing only nitrate, nitrate was recovered to 100% in a 30 h dark experiment but nitrate decomposition was only observed under irradiation and reached 2% after 30 h reaction time. For the nitrate/titania system in the dark, the amount of nitrate adsorption reaches 10.0% on TELE and 7.5% for both TVA and TAA exceeding that of Degussa P25 (2.0%). The performances of all catalysts toward nitrate reduction under UV irradiation that lasted up to 13 h showed a variation in activity when either P25 or composite titanias (Fig. 5) were used. All mesoporous catalysts and the P25 achieved, respectively ca. 60–45% and 7% conversions within 13 h reaction time. This is rather surprising given that previous reports suggest that TiO_2 on its own is either inactive [19] or slightly active in the photocatalytic

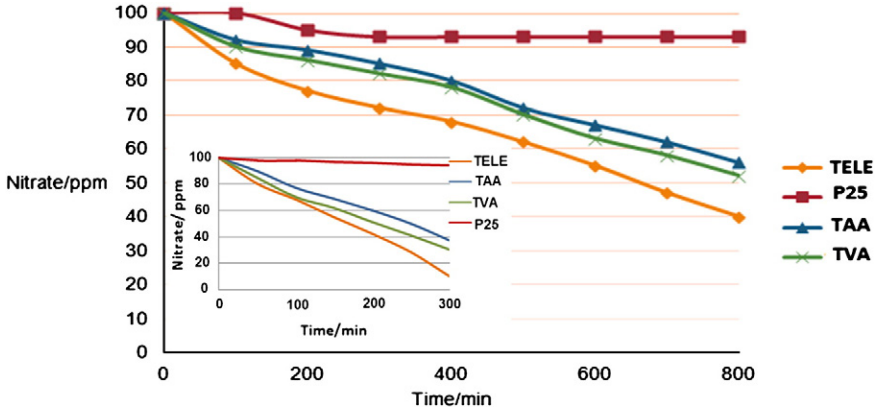

Fig. 5. UV-degradation profile of 100 ppm nitrate as a function of irradiation time in the presence of P25 and mesoporous composite titania catalysts in the absence of any hole scavengers where the in-set figure illustrates when 0.06 M formic acid is used as hole scavenger.

removal of nitrates [20]. Perceiving such high activity in the absence of any hole scavenger let us presume that residual organic moieties can act as hole scavenger to contribute to the apparent activity. In concordance, the TGA diagram of TELE (not shown) evidences the presence of residual organic template at 350 °C. Differences in photocatalytic behavior as a function of particle size are often related to differences in adsorbability and it has been suggested [21] that sufficient time should elapse before monitoring photocatalytic activity to eliminate the effect of adsorption. Thus, prior to illumination, the catalysts were introduced to the nitrate ion solution and left for 60 min for assuring that the surfaces have reached a stable equilibrated state with their surroundings. In this context, it has been revealed from XRD and TEM investigations that TELE possesses lower particle diameter than TVA and TAA assuming that crystallite size could have a decisive influence on the activity. In addition, TELE possessed high surface areas and pore volumes than rest of samples including P25 highlighting an explicit role for mesoporous architecture and texturing on the activity. Besides, the lattice-matched anatase/TiO_2(B) heterojunction structure (see Fig. 2) on the atomic level can remarkably suppress photogenerated charge carrier recombination. Accordingly, based on the above mentioned information, one can devote the increase in activity for mesoporous titanate to the presence of anatase/TiO_2(B) junction nevertheless exceeding the activity of TELE comparatively advocates that 61.4% anatase and 33.3% TiO_2(B) with minor amount of rutile comprised of 5.3% constitute the most active catalyst. It can be seen that the decrease in activity from 50% in TVA to 45% in TAA is not comparable to the decrease in anatase from 58% to 32% emphasizing that there must be other factors affecting the activity such as particle size and rutile percentages that if it exceeds 5% it influences the activity as in TVA (20%) on which quicker electron–hole recombination rate can take place.

3.4. The effect of hole scavenger

Formic acid with a simple one carbon molecular structure was chosen as a hole scavenger to investigate its effect on nitrate reduction. The activity data attained for TELE (see Supplementary data) confirms that high conversion was obtained with formic acid concentration range from 0.02 to 0.08 mol dm^{-3}, above which lower conversions were observed. Fig. 5-inset shows UV-degradation profile of 100 ppm nitrate as a function of irradiation time for all samples in the presence of 0.06 mol dm^{-3} formic acid. An average activity of 253 μmol $min^{-1}g_{cat}^{-1}$ was achieved for TELE (equivalent to 91% conversion) in the presence of formic acid after 5 h of irradiation where TAA, TVA and P25 achieved 202, 186 and 25 μmol $min^{-1}g_{cat}^{-1}$ comparable respectively, to 73%, 67% and 6% conversions. Addition of formic acid increases the photoactivity of TELE by more than 30% conversion; from 60% in the absence of acid to 91% in its presence, and rather reduces the time into 5 h.

The photocatalytic H_2-production activity over mesoporous composite titania catalysts with 10 vol.% formic acid solution was measured under UV–light irradiation, as shown in Fig. 6. Among all the prepared photocatalysts, TELE showed highest activity towards production of the hydrogen gas. The activity was found to be almost the same in two repeated runs confirming the stability of the photocatalysts. For comparison study, we have tested the photocatalytic activity towards hydrogen generation over all the photocatalysts without taking any sacrificial agent and it has been found that they were able to produce lower amounts comparatively emphasizing the role of residual organic moieties as sacrificial agents.

Raising the temperature into 773 K decreases the activity of TELE in the presence of HCOOH into 10% conversion due to decreasing the TiO_2(B) content into 7% in favor of rutile (from 5 into 31%) and this evidences the importance of TiO_2(B) on the activity together with anatase as a synergy system. The selectivity of nitrate photoreduction in the presence of HCOOH for TELE catalyst was investigated (see Supplementary data) and thus indicated small amounts of ammonia (5%) and nitrite (20%) as products. From the experimental results, it is clear that TiO_2(B)/anatase at intermediate percentages of TiO_2(B) at 33.3% and anatase concentrations at 61.4% function more effectively as a separation center. Presumably, the reduced efficiency at the highest TiO_2(B) concentration of 40–48% might result from ineffective charge transfer at the interface between TiO_2(B) and anatase.

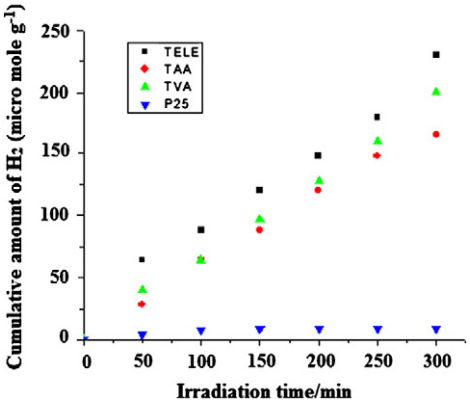

Fig. 6. Changes in H_2 concentration as a function of irradiation time in the presence of formic acid as a sacrificial agent for P25 and mesoporous composite titania catalysts.

4. Conclusions

The results presented confirm the potential of heterojunction anatase/TiO_2(B) photocatalyst for removal of nitrates from polluted water. Factors including TiO_2 morphology and hole scavenger were identified as being relevant parameters. The photocatalytic activities were maximized on mesoporous titanates of TiO_2(B)/anatase composite greater than that on P25 with improved selectivities. It was found that the suitable amount of the TiO_2(B) (~33%) effectively increases the photo-activity of the TiO_2 surface that behaves as sites where electrons accumulate. The experiments demonstrated that the residual organic templates played a marked role in enhancing the activity in the absence of any hole scavenger. Nitrate was effectively degraded in aqueous TiO_2(B)/anatase suspension by more than 90% within 5 h.

Acknowledgment

Authors are indebted to King Abdul Aziz City for Science and Technology (KAST) for funding the project number LGP-13-15 from which this work is produced.

References

[1] W.J. Williams, Handbook of Anion Determination, Butterworth, London, 1979.
[2] World Health Organization, International Standards for Drinking Water, 3rd edn, Springer-verlag, Geneva, 1971.
[3] H. Kominami, T. Nakaseko, Y. Shimada, A. Furusho, H. Inoue, S. Murakami, Y. Kera, B. Ohtani, Chemical Communications (2005) 2933–2937.
[4] H. Kominami, A. Furusho, S. Murakami, H. Inoue, Y. Kera, B. Ohtani, Catalysis Letter 76 (2001) 31–36.
[5] A. Kudo, K. Domen, K.-I. Maruya, T. Onishi, Journal of Catalysis 135 (1992) 300–307.
[6] K.T. Ranjit, T.K. Varadarajan, B. Viswanathan, Journal of Photochemistry and Photobiology A: Chemistry 89 (1995) 67–74.
[7] B. Bems, F.C. Jentoft, R. Schlögl, Applied Catalysis B: Environmental 20 (1999) 155–163.
[8] H. Zhang, G.R. Li, L.P. An, T.Y. Yan, T.Y. Gao, X.P. Zhu, Journal of Physical Chemistry C 111 (2007) 6143–6150.
[9] M.D. Wei, Z.M. Qi, M. Ichihara, I. Honma, H.S. Zhou, Chemical Physics Letters 424 (2006) 316–323.
[10] J.C. Lee, T.G. Kim, H.J. Choi, Y.M. Sung, Crystal Growth and Design 7 (2007) 2588–2592.
[11] D.-L. Shieh, C.-H. Ho, J.-L. Lin, Microporous and Mesoporous Materials 109 (2008) 362–369.
[12] M.V. Koudriachova, Journal of Nano Research 11 (2010) 159–164.

[13] A.R. Armstrong, G. Armstrong, J. Canales, R. García, P.G. Bruce, Angewandte Chemie, International Edition 43 (2004) 2286–2291.
[14] T. Hongo, A. Yamazaki, Microporous and Mesoporous Materials 142 (2011) 316–323.
[15] B.L. Bischoff, M.A. Anderson, Chemistry of Materials 7 (1995) 1772–1777.
[16] W. Li, C. Liu, Y. Zhou, Y. Bai, X. Feng, Z. Yang, L. Lu, X. Lu, K.-Y. Chan, Journal of Physical Chemistry C 112 (2008) 20539–20545.
[17] L. Raboin, J. Yano, T.D. Tilley, Journal of Catalysis 285 (2012) 168–176.
[18] Y.M. Lin, Y.H. Tseng, J.H. Huang, C.C. Chao, C.C. Chen, I. Wang, Environmental Science & Technology 40 (2006) 1616–1621.
[19] M.M. Mohamed, M.M. Al-Esaimi, Journal of Molecular Catalysis A: Chemical 255 (2006) 53–61.
[20] M.M. Mohamed, W.A. Bayoumy, M. Khairy, M.A. Mousa, Microporous and Mesoporous Materials 103 (2007) 174–182.
[21] F. Zhang, R. Jin, J. Chen, C. Shao, W. Gao, L. Li, N. Guan, Journal of Catalysis 232 (2005) 424–432.